View Online / Journal Homepage
Dynamic Article Links

Lab on a Chip

Cite this: DOI: 10.1039/c2lc40154a

www.rsc.org/loc

PAPER

Nanowire-integrated microfluidic devices for facile and reagent-free mechanical cell lysis†

Jung Kim,[a] Jung Woo Hong,[b] Dong Pyo Kim,[c] Jennifer H. Shin[b] and Inkyu Park*[a]

Received 13th February 2012, Accepted 14th May 2012
DOI: 10.1039/c2lc40154a

Cell lysis is an essential task for the detection of intracellular components. In this work, we introduce novel microfluidic devices integrated with patterned one-dimensional nanostructure arrays for facile and high-throughput mechanical cell lysis. The geometry of the hydrothermally grown ZnO nanowires, characterised by sharp tips and high aspect ratios, aids in anchoring the cell and tearing the plasma membrane, enabling simple and highly efficient extraction of cellular proteins and nucleic acids. This method lyses cells more effectively than conventional chemical lysis methods with simpler equipment and a shorter processing time.

Introduction

Cell lysis is an essential step for the extraction of intracellular components such as organelles, proteins, and nucleic acids.[1] A number of different approaches for cell lysis have been developed, including chemical,[2–4] mechanical,[5–7] electrical,[8,9] optical [10] and acoustic [11] methods. The most well-established and well-known lysis method is chemical lysis, which uses a detergent to weaken the cell membrane.[1] This method does not require specialised equipment and can be applied to both adherent and suspended cells. However, the detergent used in chemical lysis may result in protein denaturation. Electrical, optical and acoustic methods are less harmful to cells, but they require specialised or expensive instruments, such as electrical circuits, power supplies, laser systems, or sonicators, to stimulate and lyse the cells. Recently, a number of methodologies based on microfluidic channels have been actively developed for applications in lab-on-a-chip systems.[12] Mechanical cell lysis based on a microfluidic platform is much simpler than the aforementioned approaches because it relies on the mechanical forces induced by the physical interaction between the cells and the structures within the microfluidic device. In particular, nanoscale structures can mechanically stimulate cells to effectively induce disruption of cellular membranes (*i.e.*, lysis) and release of intracellular components. Using a deep reactive ion etching (DRIE) method, Di Carlo *et al.* fabricated silicon nanobarbs to lyse HL-60 and whole blood cells in a microfluidic channel.[5] Yang *et al.* also used silicon nanobarbs, fabricated by anisotropic wet etching, to make microfluidic chips for the mechanical lysis of EL4 mouse T-lymphoma cells in a handheld device.[13] Mechanical lysis methods based on microfluidic platforms are more effective than conventional chemical, ultrasonic, or electrical lysis methods without the need for chemical agents, power sources, or bulky equipment. However, in these previous studies, the fabrication of nanostructures within microchannels required expensive equipment and/or stringent process control.

In this paper, we introduce a novel microfluidic device for mechanical cell lysis. This device features ZnO nanowires that can be easily synthesised using an eco-friendly, inexpensive, and facile hydrothermal reaction. The hydrothermal synthesis of mechanically robust ZnO nanowires can be achieved at low temperatures (80–95 °C) and low atmospheric pressure in a mild chemical environment. The control of structural parameters such as height, aspect ratio, and tip geometry can be easily attained by adjusting the synthesis chemistry, temperature, and duration. In this work, we utilise the geometric and mechanical properties of ZnO nanowires for mechanical cell lysis. The geometric properties of ZnO nanowires include high aspect ratios and small tip radii, whereas the mechanical properties include a high Young's modulus (~140 GPa) and strength (~7 GPa).[14] ZnO nanowires were fabricated within microfluidic channels by hydrothermal synthesis. Then, effective cell lysis was confirmed for multiple cell types by qualitative analysis (*via* fluorescence microscopy) and quantitative analysis (*via* spectrophotometry of intracellular proteins and nucleic acids). We have experimentally verified that highly efficient cell lysis can be achieved by simply passing the cells through the nanowire-integrated microfluidic channel. We have also found that performance is significantly affected by the arrangement of nano and micro/nano hybrid structures. By quantifying the released intracellular protein and nucleic acid in the cell lysate, we compared our novel mechanical lysis device

[a]*Multifunctional and Integrated Nanosystem Technology (MINT) Group, School of Mechanical, Aerospace and Systems Engineering, Division of Mechanical Engineering, KAIST, 291 Daehak-ro, Yuseong-gu, Daejeon, Korea. E-mail: inkyu@kaist.ac.kr; Fax: +82 42 350 3210; Tel: +82 42 350 3233*
[b]*Soft Biomechanics and Biomaterials Laboratory, School of Mechanical, Aerospace and Systems Engineering, Division of Mechanical Engineering, KAIST, 291 Daehak-ro, Yuseong-gu, Daejeon, Korea*
[c]*National Creative Research Center of Applied Microfluidic Chemistry, Department of Chemical Engineering, POSTECH, Pohang, Korea*
† Electronic supplementary information (ESI) available. See DOI: 10.1039/c2lc40154a

using ZnO nanowires to a conventional chemical lysis method. The results show that our device performs as well as or better than conventional methods but uses much simpler process and equipment.

Experimental

Fabrication of ZnO nanowire arrays within microfluidic channels

Cell lysis devices utilising nanowire arrays were fabricated by two different methods. First, an *in situ* synthesis method described in our previous work [15] was used to fabricate nanowire arrays. In order to make ZnO nanowire arrays in zigzag dot or wedge patterns for cell lysis, the ZnO seed layer was patterned by UV photolithography, followed by e-beam evaporation of Cr/ZnO thin films (Cr = 10 nm, ZnO = 30 nm thick) and a lift-off process onto a glass wafer. A polydimethylsiloxane (PDMS) microchannel (height: 20 μm, width: 150 μm) was prepared by a conventional replication technique that uses SU-8 patterns as a master mould. The PDMS microchannel was aligned and then bonded to the glass substrate with a patterned ZnO seed layer. For the synthesis of nanowires, precursor solution [zinc nitrate hexahydrate, $Zn(NO_3)_2{\cdot}6H_2O$, 98%, Sigma Aldrich], hexamethylenetetramine (HMTA, $C_6H_{12}N_4$, 99+%, Sigma Aldrich) and polyethylenimine [PEI, $(C_2H_5N)_n$, Sigma Aldrich, in deionised (DI) water][16] was flown through the PDMS microchannel by two syringe pumps (infusing and withdrawing pumps) at a continuous flow rate (1 μL min^{-1}) while the glass substrate was heated on a heating plate at 95 °C. After 30–160 min of synthesis, the microchannel was rinsed by flowing DI water (flow rate = 5 μL min^{-1}) through the channel at room temperature. Finally, the sample was thermally annealed on a hotplate at 95 °C while air flowed through the microchannel at a flow rate of 5 μL min^{-1} for 120 min. This procedure is depicted in Fig. 1 (a).

Another approach for nanowire fabrication was based on a well-known ZnO hydrothermal synthesis method in the bulk phase,[16] but was performed within a PDMS microchannel containing three dimensional microstructures. Here, various micropost arrays (cross-sectional area = 15 μm × 15 μm, height = 20 μm) were arranged in a microchannel (width = 200 μm, height = 20 μm) in the following layouts: (a) a uniform array of 3(4) × 28 microposts with a gap of 40 μm (hereafter, "UG_1", Fig. S1 (a)†), (b) a uniform array of 5 × 40 microposts with a gap of 25 μm, (hereafter, "UG_2", Fig. S1 (b)†), (c) a non-uniform array of 3(4) × 10 (gap = 40 μm), 4(5) × 10 (gap = 30 μm) and 5(6) × 10 (gap = 20 μm) microposts with decreasing downstream gaps (hereafter, "DG_1", Fig. S1 (c)†), and (d) a non-uniform array of 3(4) × 12 (gap = 40 μm), 4(5) × 10 (gap = 30 μm) and 5(6) × 3 (gap = 20 μm) microposts with decreasing downstream gaps (hereafter, "DG_2", Fig. S1 (d)†). The total length of the micropost array within the channel was identical (L = 1.5 mm), regardless of the design layout (See Fig. S1 in the supporting information†). These PDMS microchannels containing different micropost arrays were also fabricated by SU-8 photolithography followed by the PDMS moulding technique mentioned above. The microchannel side of the PDMS block was coated with a few drops of ZnO nanoparticle seed solution [zinc acetate dehydrate, $Zn(CH_3COO)_2{\cdot}2H_2O$, 99.0%, JUNSEI] and sodium hydroxide (NaOH, 97%, DAEJUNG, in methanol). When the seed solution started to evaporate, the channel was rinsed with ethanol. This seeding step was repeated three times to form a uniform and dense layer of nanoparticle seeds. Then, the PDMS block was annealed at 150 °C for 20 min. For the selective synthesis of ZnO nanowires along the microchannel, a thin PDMS layer (thickness <1 μm) was coated on the surface of the outside of the microchannel and cured at room temperature (20 °C) for 24 h. ZnO nanowires were synthesised on the seeded PDMS microchannel by a hydrothermal reaction at 95 °C for 2 h. The PDMS block was then

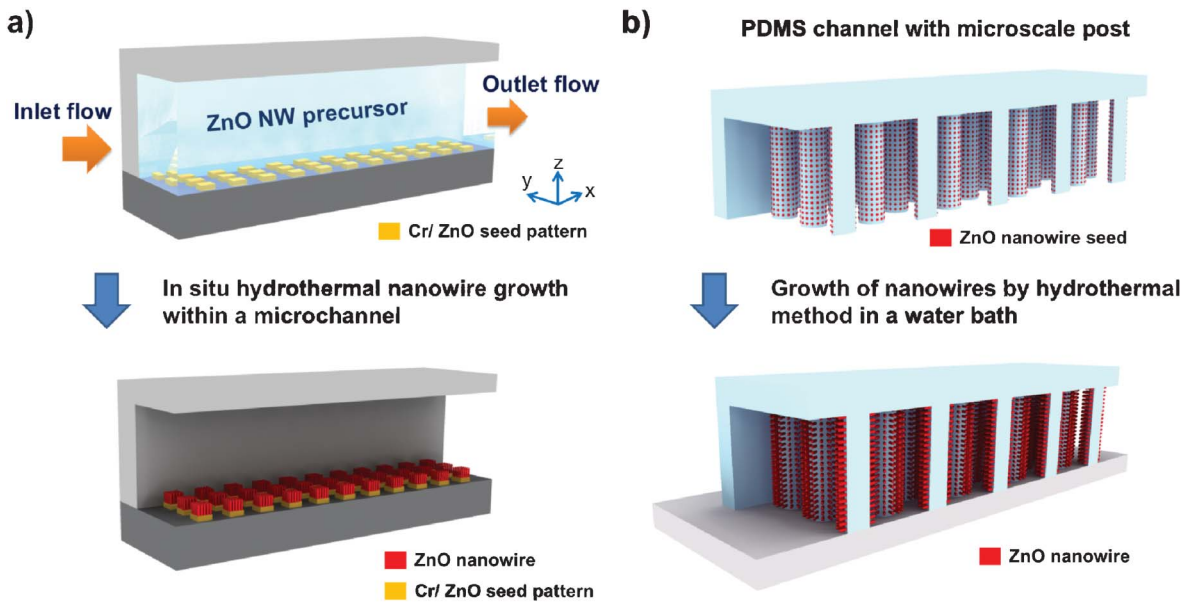

Fig. 1 Schematic diagram of (a) patterned growth of ZnO nanowire arrays by an *in situ* synthesis method and (b) growth of ZnO nanowires on microstructure arrays by a conventional hydrothermal method.

rinsed with DI water and blown dry with air. It was then bonded to the glass substrate by a stamp-and-stick method.[17]

Cell preparation

Three different cell types were used in this study. All three cell lines, immortalised human keratinocytes (HaCaT, a gift from Amore Pacific Corporation), HeLa (ATCC, CCL-2) and Jurkat (ATCC, TIB-152), were cultured at 37 °C in a 5% (v/v) CO_2 incubator. HaCaT and HeLa cells were maintained in Dulbecco's modified Eagle's medium (DMEM, Gibco) supplemented with 10% (v/v) FBS (Gibco) and 1% (v/v) penicillin-streptomycin (Gibco), while Jurkat cells were maintained in Roswell Park Memorial Institute medium (RPMI, Gibco) and were also supplemented with 10% (v/v) fetal bovine serum (FBS) and 1% (v/v) penicillin-streptomycin. All cells were cultured for 4 days prior to the experiment. Just before the lysis experiment, the cells were detached from the culture dish using trypsin-EDTA (Gibco) and suspended in Dulbecco's phosphate-buffered saline (DPBS, Gibco).

Cell lysis and qualitative analysis by actin filament dyeing with rhodamine-phalloidin

HaCaT cells were flown through the microchannel at a concentration of 800 cells μL^{-1} in DPBS solution at a flow rate of 5 $\mu L\ min^{-1}$. In order to confirm cell breakage, a diluted solution of Alexa Fluor® 568 phalloidin (Invitrogen) was mixed with the cell solution, allowing for visualisation of fluorescently labelled actin filaments in the event of cells mechanically rupturing. Intact cells do not allow the phalloidin to pass through the cell membrane to label actin filaments. Therefore, this method can be used as a simple but easily visible indicator of the cell lysis. Cells were examined under a fluorescent microscope (Axiovert 200 M, Carl Zeiss).

Quantitative analysis by measurement of intracellular protein and nucleic acid concentrations

Suspensions of cells (5000 cells μL^{-1}) subjected to mechanical lysis in the microchannel for 5 min at the aforementioned rate were collected at the outlet. As a positive control for mechanical lysis, chemical lysis was also conducted by mixing suspended cells with a passive lysis buffer (Promega) supplemented with a protease inhibitor cocktail (Roche) and incubated in ice for 30 min. Cell suspensions of 100 μL, either mechanically or chemically lysed, were centrifuged at 12 000 rpm for 10 min, and concentrations of intracellular protein and nucleic acids were determined using a spectrophotometer (NanoDrop 1000, Thermo Scientific NanoDrop™). The absorbance of intracellular proteins and nucleic acids in 2 μL of sample solutions was measured at wavelengths of λ = 280 nm and λ = 260 nm, respectively. The optical absorbance of protein is commonly measured at λ = 280 nm to identify amino acids such as tryptophan, tyrosine and cysteine. The absorbance of proteins may differ according to the relative concentrations of these three amino acids. The absorbance values from the spectrophotometer are automatically processed to obtain the total protein concentration in the sample. The absorbance at λ = 260 nm represents the total nucleic acid concentration, including double-stranded DNA, single-stranded DNA and RNA.

Results

Nanostructure fabrication

Fig. 2 (a) shows the nanowire array fabricated by an *in situ* synthesis method (hydrothermal growth within a pre-fabricated microchannel). As shown in the SEM images, nanowires were grown only on patterned sites. The height of the nanowire array can be controlled by changing the synthesis time.[15] Although many nanowires grew vertically from the substrate, a significant number of nanowires grew at tilt angles of 15–45° from a normal direction. Randomly oriented nanowires may provide more chances for the cells to encounter the tip of nanowires. Thus, the tilt angle is one of the important geometric factors affecting cell lysis. The nanowires with a large deviation from the normal to the substrate (the bottom of microchannel) are presumed to anchor cells more effectively. The length of the nanowires is also an important factor in the efficiency of cell lysis because it determines the space available to the cells as they travel between the ceiling of the microchannel and the nanowire array. If the travelling gap is small, there are more chances for the cells to interact with nanowires. On the contrary, too small a gap between the ceiling and nanowires may hinder the flow of cells, leading to clogging of lysed cells. For the lysis experiment with arrays of *in situ* grown nanowires, the synthesis of nanowires was conducted for 1 h to obtain 2–3 μm long nanowires within 20 μm high microchannels. Fig. 2 (b) shows nanowires grown on the microchannel with the micropost array (hereafter, "MP_NW microchannel") using conventional bulk-phase hydrothermal synthesis. ZnO nanowires were uniformly grown on the sidewalls of the microchannel and the microposts. No nanowires were grown on the top surfaces of the microposts because they were covered with a thin PDMS layer during the seed passivation step. Nanowires also did not grow at some locations around the micropost array and sidewalls of the microchannel, which can be attributed to the non-uniform coating of ZnO nanoparticle seeds

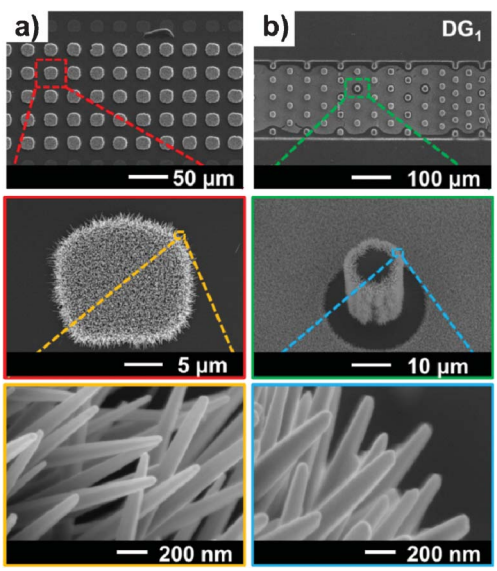

Fig. 2 SEM images of (a) an *in situ* grown nanowire array by hydrothermal reaction within pre-fabricated microchannel and (b) nanowires on a micropost array that were hydrothermally grown in the bulk phase, followed by microchannel packaging.

due to the poor wetting of seed solution at these concave corners of PDMS. For the cell lysis, we used the microchannel with ~2 μm long nanowires on the micropost array. Because nanowires on microposts were grown using nanoparticle seeds, they were also tilted from the normal direction of the micropost surfaces.

Although the stiffness and ultimate strength of ZnO nanowires is high, their physical adhesion to the PDMS substrate is not very robust. Therefore, partial delamination of ZnO nanowires from the PDMS substrate can be observed by harsh blowing with compressed air or with water jet. However, the adhesion is still strong enough to endure shear stress due to the fluid flow and normal stress by cell collision during cell lysis. From the optical micrograph and SEM images, we could not observe any detachment of nanowires during and after the cell lysis experiment.

Cell lysis and qualitative analysis of cell lysis performance

Fig. 3 (b) shows the interaction of a single HaCaT cell (diameter = 20 μm) with the nanowire array (gap = 15 μm), visualised using an optical microscope. We flew the cell solution through the microchannel using a pair of syringe pumps (one for injection at the inlet and another for withdrawal at the outlet) as described in Fig. 3 (a). Over time, we could observe the cells anchoring on the nanowire array, being stretched by the shear force of the flow, and then bursting. In Fig. 3 (b), a two-dimensional image of the boundary of a cell is marked for improved visualisation. An initially round cell stretches and flattens to a larger projected area as it experiences the flow's shear force (Fig. 3 (b),(c)). For improved visualisation of the cell-nanowire interaction, the readers can refer to the video clip in the Supporting Information.† Although it is difficult to differentiate whether

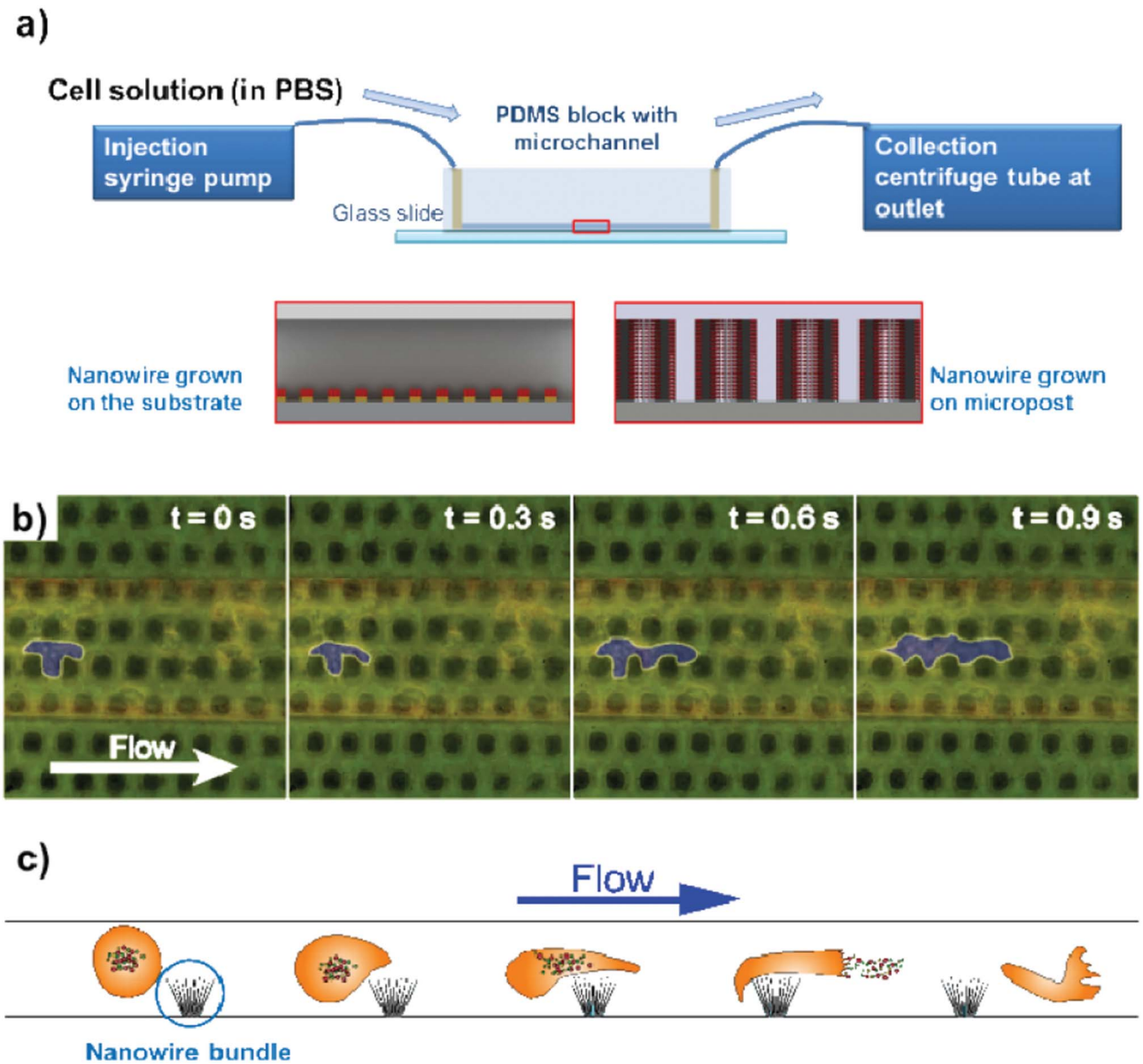

Fig. 3 (a) Experimental setup of cell lysis, (b) visualisation of the deformation of single a HaCaT cell by nanowire arrays: captured images of cell deformation by the nanowires in the microchannel and (c) the mechanism of cell deformation and lysis by the nanowire array.

the cell was completely ruptured or partially damaged, we could confirm that the cells experienced a strong physical interaction with the arrays of nanowire bundles. Because nanowires feature sharp tips pointing out at random orientations, they provide a large surface area for easy anchoring of cells and initiation of mechanical lysis. The cell then continues to stretch under shear flow and experiences a stress over its ultimate strength, causing the rupture and release of intracellular materials (Fig. 3 (c)). In order to determine whether the cell membrane was ruptured or just deformed, we directed Alexa Fluor® 568 phalloidin along with HaCaT cells through the nanowire-integrated microchannel. In the case of cell rupture, intracellular materials would be released from the cells and extracellular materials could be transferred into the cells. Phalloidin molecules in Alexa Fluor® 568 phalloidin bind to actin filaments at the interface between adjacent actin subunits and emit red fluorescent light (peak wavelength = 568 nm). Because phalloidin molecules cannot permeate cell membranes, actin filaments cannot be labelled unless cells are ruptured or mechanically damaged. By observing the light emission from the labelled actin filaments, mechanical cell lysis can be qualitatively verified. Fig. 4 shows the fluorescence images after the HaCaT cells mixed with Alexa Fluor® 568 phalloidin were directed through the PDMS microchannels featuring nanowire arrays of different patterns (zigzag, wedge and nanowires on micropost array) or an empty microchannel. The light emission from a phalloidin-labelled actin filament is clearly observed from the nanowire-integrated microchannels while no light emission is observed from the empty microchannel without nanowires. This result proves that cell lysis was successfully achieved, allowing the phalloidin molecules to enter into the cells. The cell lysis efficiency of various nanowire configurations can be qualitatively compared by observing the intensity of fluorescent light emission from different configurations. The total amount of fluorescence appears to be greater in the MP_NW microchannel, where the red fluorescence is spread across the entire channel, than in the microchannel with the nanowire array grown on the substrate, where only a few red spots are visible. This result proves that the MP_NW microchannels more effectively lyse cells than other microchannels. Here, nanowires are grown in all directions along the sidewalls of microposts. As cells travel through the microchannel, many cells can collide against the sidewalls of the micropost array. Upon collision, cells are anchored to the nanowires as explained above, and the fluid flow drives the shear deformation of cells. Moreover, the height of microposts is designed to be identical to that of microchannel, allowing the cell-nanowire interaction to occur throughout the entire depth of microchannel. If nanowires were to be grown from the substrate with lengths of 2–3 μm, the mechanical interaction between the cells and the nanowires would be limited because the nanowires could interact only with the bottom of the cells. Although the length of nanowires can be extended beyond 10 μm, synthesis would require a long period of time (>10 h). Therefore, we have concluded that the MP_NW microchannel provides a much more convenient route for efficient cell lysis due to its hierarchical micro/nanostructures.

Quantitative measurement of cell lysis performance

Because the MP_NW microchannels were shown to improve cell lysis, we used this configuration for further quantitative analysis. The effect of the geometrical parameters of the micropost array (gap size and pattern uniformity) on the cell lysis efficiency was analysed. Quantitative analysis was conducted with the spectrophotometer by measuring the concentrations of intracellular proteins and nucleic acids from cell suspensions after mechanical lysis. At first, the lysis performance was examined on microchannels featuring two different, yet uniform, inter-post spacings (G) (UG_1: G = 40 μm and UG_2: G = 25 μm) as shown in Fig. 5 (a). The concentrations from MP_NW microchannels were higher than the empty microchannel by 1.3 (UG_1) and 1.8 (UG_2) times for intracellular proteins and by 2.2 (UG_1) and 3.2 (UG_2) times for nucleic acids, respectively. The UG_2 microchannel showed higher concentrations of both protein and nucleic acid than the UG_1 microchannel. This result can be explained by comparing the inter-post spacing to the cell size. For UG_2, the inter-post spacing (G) was 25 μm and the average length of the nanowires on the sidewalls of the micropost

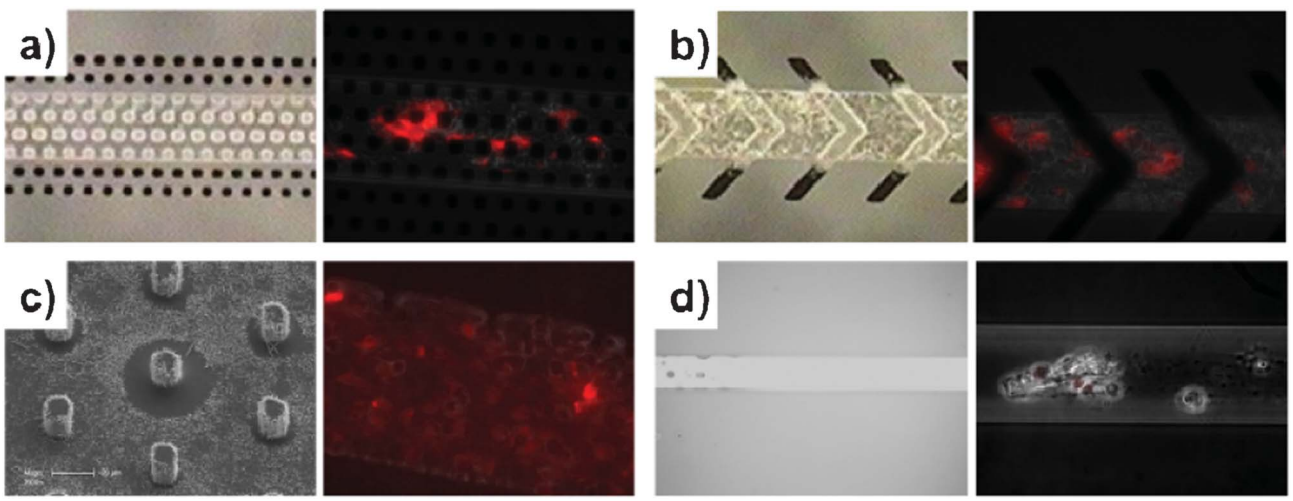

Fig. 4 Visualisation of cell lysis performance in the microchannel depending on the nanowire arrays of different designs ((a) zigzag pattern, (b) wedge pattern and (c) nanowires on the micropost array) and (d) in an empty microchannel by actin filament dyeing with Alexa Fluor® 568 phalloidin.

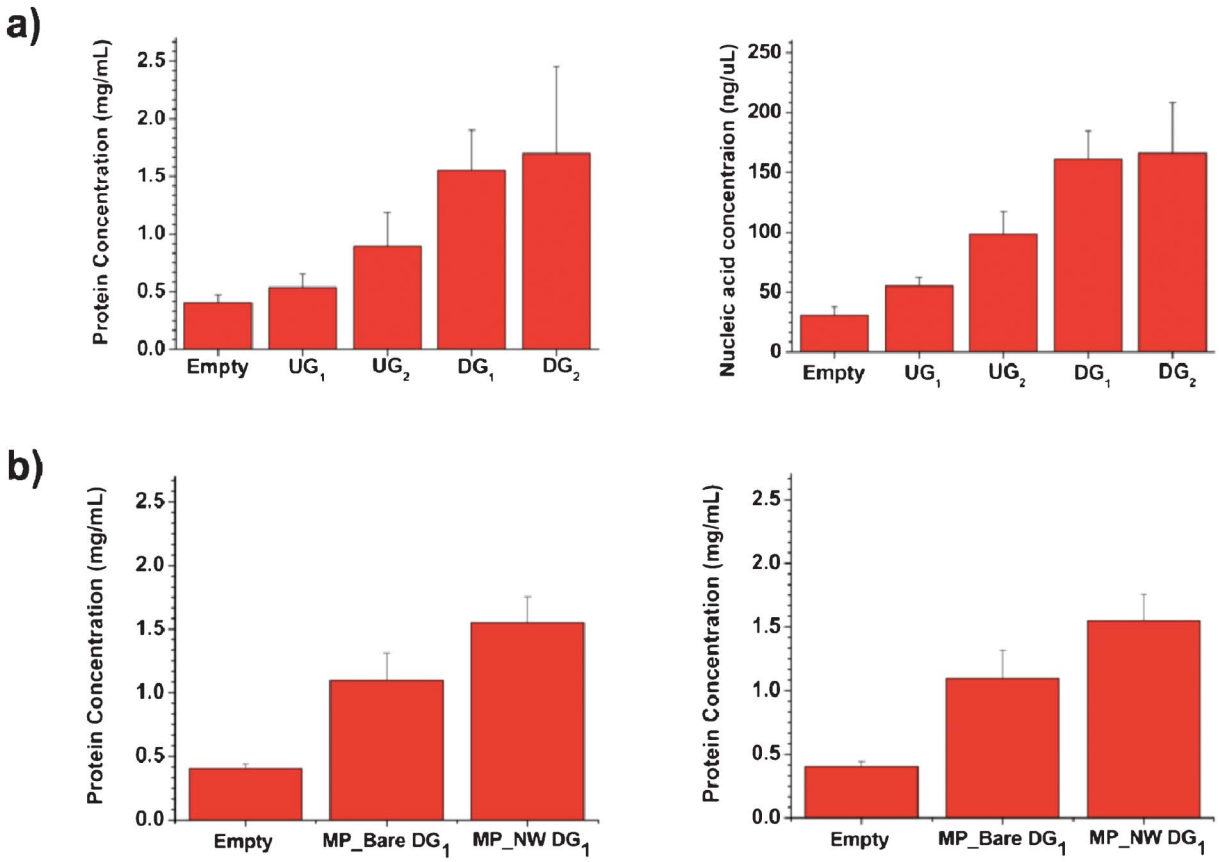

Fig. 5 Protein and nucleic acid concentrations of lysed HaCaT cells after flowing through (a) empty and MP_NW microchannels with different layouts (UG_1, UG_2, DG_1, and DG_2) and (b) empty channels, channels with microposts only, and MP_NW channels with a DG_1 layout. Error bars represent the mean standard error (SE).

($L_{nanowire}$) was 2 μm. Thus, the average gap was ~21 μm, which is comparable to the average diameter of HaCaT cells (D_{HaCaT} = 20 μm). On the other hand, for UG_1, because G = 40 μm and $L_{nanowire}$ = 2 μm, the average gap is 36 μm, which is ~1.8 times larger than the average diameter of HaCaT cells.

A numerical flow simulation by COMSOL™ (Fig. S2†) reveals that the streamline is uniform for micropost arrays with a uniform gap (UG_1 and UG_2), which may be the reason for the limited probability of collision between cells and nanowire-integrated microposts. In order to enhance the probability of a cell-micropost interaction, the array of microposts was re-designed with gaps decreasing in the downstream direction (DG_1 and DG_2). The numerical flow simulation shows more complex streamlines for DG_1 and DG_2 compared to UG_1 and UG_2. As shown in Fig. 5(a), the average protein concentrations from DG_1 and DG_2 were 3.8 and 4.2 times higher than those from the empty channel, respectively. Also, the average nucleic acid concentrations from DG_1 and DG_2 were 5.3 and 5.4 times higher than those from the empty channel, respectively. Compared to UG_1 and UG_2, both DG_1 and DG_2 exhibited enhanced extraction of both protein and nucleic acid from cells. Table S1 shows a summary of the protein and nucleic acid concentrations from different microchannels.† Among the different designs, the DG_2 microchannel was found to lyse cells the most effectively with the largest intracellular protein and nucleic acid concentrations detected by spectrophotometry.

We evaluated the protein and nucleic acid concentration data using Student's t-test. The cell lysis efficiency of the nanowire-integrated microposts (DG_1 microchannel) is significantly greater than the empty microchannel with p-values of 0.0054 for proteins and 0.0013 for nucleic acids of lysate samples, respectively. The comparison between UG_1 and DG_1 (p = 0.0143 for proteins and p = 0.0091 for nucleic acids) indicates a significant improvement in performance after rearranging the micropost configuration. Generally, with an increase in complexity in both the arrangements and structures, we obtain better yield of both proteins and nucleic acids (Fig. 5). Also, as the inter-post spacing becomes smaller, the lysis performance is improved. However, our Student's t-test results indicate that the differences between some of these data are not statistically significant, probably because the increased complexity of the structures results in higher standard deviations. However, the enhancement of cell lysis by nanowire-integrated microposts can still be inferred by comparing the average yields of protein and nucleic acid.

We also examined the released protein and nucleic acid concentrations of the lysed cell suspensions that passed though the microchannels with a bare micropost array (*i.e.*, without nanowires grown, hereafter, "MP_BARE"). These microchannels also provide higher concentrations of protein and nucleic acid than empty microchannels, indicating that cells can be ruptured by collision against the walls of bare microposts and by

fluid shear along a dense array of microposts. However, cell lysis efficiency was enhanced using MP_NW microchannels, as shown in Fig. 5 (b). For the DG_1 layout, nanowire integration on microposts resulted in a 41% increase in released protein and a 48% increase in released nucleic acid. Although the p values between MP_NW and MP_BARE from the Student's t-test are large ($p = 0.3882$ for DG_1 in the case of protein), higher average protein and nucleic acid concentrations for MP_NW compared to MP_BARE indicate the efficiency of nanowires for the cell lysis. As mentioned above, large p values can be attributed to the structural variability of nanowires and the complexity of cell-nanowire interaction. However, by comparing the empty and MP_NW microchannels, it can be concluded that excellent cell lysis was achieved through the synergy of micropost arrays and nanowires grown along the microposts.

We also studied the versatility of nanowire-integrated microchannels for the mechanical cell lysis of various cell types: HaCaT (average diameter, $D \approx 20$ μm), HeLa ($D \approx 15$ μm) and Jurkat ($D \approx 10$ μm) cells. As shown in Fig. 6, the cell lysis in MP_NW microchannels was higher than in empty microchannels for all cell types. A significant improvement in cell lysis can be obtained with a DG_1 microchannel for all three cell types (HaCaT, HeLa and Jurkat) compared to the empty microchannel. For example, the protein concentrations for HeLa cells were 1.678 mg mL^{-1} for the DG_1 microchannel as compared to 0.377 mg mL^{-1} for the empty microchannel.

We also compared the cell lysis in MP_NW microchannels (DG_1) to cell lysis *via* a conventional chemical lysis method (Fig. 7). In the case of HaCaT cells, MP_NW microchannels show higher intracellular protein concentrations (1.552 mg mL^{-1}) than with chemical lysis (0.187 mg mL^{-1}). In the case of HeLa cells, the MP_NW microchannels also show higher intracellular protein concentrations (1.678 mg mL^{-1}) than with chemical lysis. However, for the Jurkat cells, MP_NW microchannel exhibits lower intracellular protein levels than with chemical lysis [protein concentrations: 0.525 mg mL^{-1} by MP_NW microchannel (DG_1) and 1.02 mg mL^{-1} by chemical lysis]. The difference in cell lysis efficiency by MP_NW microchannels is presumed to be due to the size of cells relative to the gaps between microposts. As explained above, HaCaT and HeLa cells have average diameters of 20 μm and 15 μm, respectively. These diameters are similar to the gaps between microposts. This similarity presumably facilitated more collisions of cells with nanowires on the microposts and more anchoring and rupture of cells by fluid shear. In contrast, Jurkat cells have an average diameter of 10 μm, which is about half the gap between the microposts. Due to the small size of Jurkat cells, they can easily escape through the gaps between neighbouring microposts without collision with microposts and anchoring by nanowires. From this experiment, we have verified that MP_NW microchannels mechanically lyse cells as well as, or better than, a conventional chemical lysis method for cells of appropriate sizes. Furthermore, our mechanical lysis is a much more convenient and simple method for efficient cell lysis than the chemical lysis approach. The advantages of nanowire-integrated microfluidic devices include the following: (a) a simple lysis procedure: mechanical lysis using nanowires requires a simple setup (syringe and microfluidic chip), whereas chemical lysis requires chemicals causing protein denaturation and several post-processing steps; and (b) high throughput cell lysis: in order to obtain equivalent or greater amounts of intracellular protein and nucleic acid, only 5 min are required for the mechanical lysis, whereas more than 30 min are required for the chemical lysis.

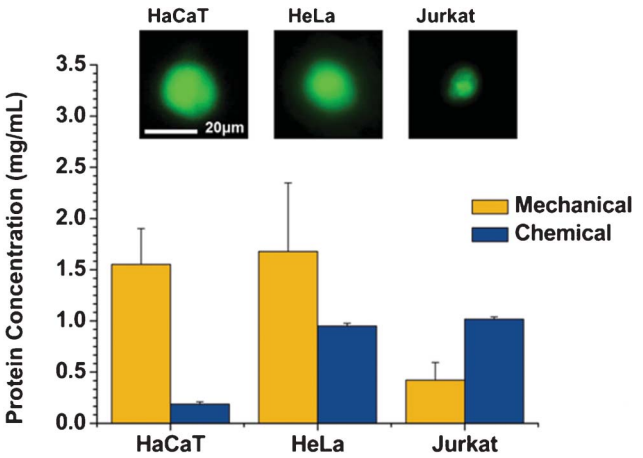

Fig. 7 Protein concentrations of lysed HaCaT, HeLa and Jurkat cells by a mechanical method utilising ZnO nanowires on microposts in microchannels and by a conventional chemical method. Error bars represent the mean SE.

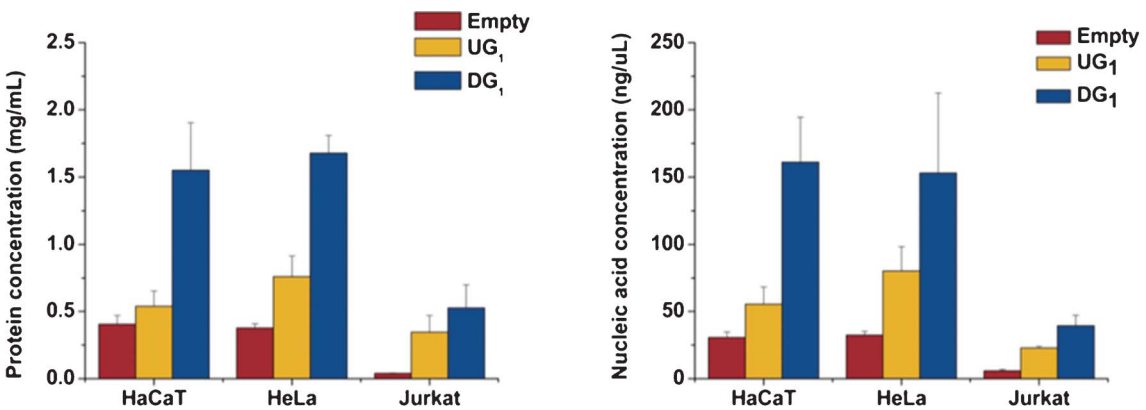

Fig. 6 Quantitative analysis of cell lysis for various cell types: (a) protein and (b) nucleic acid concentrations of lysed HaCaT, HeLa and Jurkat using an empty microchannel, a UG_1 microchannel, and a DG_1 microchannel. Error bars represent the mean SE.

Conclusion

In this paper, we proposed a simple and efficient mechanical cell lysis method utilising bottom-up synthesised ZnO nanowires integrated within microchannels. ZnO nanowires could be easily integrated into a PDMS microchannel using a low-temperature hydrothermal synthesis method. Using this device, we enabled efficient intracellular material extraction within a short period of time without the need for specialised instruments or chemicals. We could verify improved cell lysis, as compared to chemical lysis, for various cell types by detecting high yields of intracellular protein and nucleic acid. We believe that cell lysis can be further enhanced for a multitude of cells by modifying the dimensions and arrangement of the micropost array and the geometry (*e.g.*, tip size and shape) of the nanowires. Furthermore, by replacing the syringe pump with manual injection, this device enables simpler and more cost-effective lysis for the detection of intracellular components. Possible applications include simple and efficient cell sample preparation tasks for various biological downstream assays, such as biosensing or immunoassays, in lab-on-a-chip and self-diagnosis systems.

Acknowledgements

This work was supported by National Research Foundation of Korea (NRF) grants funded by the Korean government (MEST) (No 2011-0004409, 2011-0019168, and 2011-0008434). Jung Kim would like to thank Prof. Je-Kyun Park for providing HeLa and Jurkat cells and for valuable discussions.

References

1 R. B. Brown and J. Audet, *J. R. Soc. Interface*, 2008, **5**, S131.
2 M. V. Berezovski, T. W. Mak and S. N. Krylov, *Anal. Bioanal. Chem.*, 2007, **387**, 91.
3 D. Irimia, R. G. Tompkins and M. Toner, *Anal. Chem.*, 2004, **76**, 6137.
4 G. Ocvirk, H. Salimi-Moosavi, R. J. Szarka, E. A. Arriaga, P. E. Andersson, R. Smith, N. J. Dovichi and D. J. Harrison, *Proc. IEEE*, 2004, **92**, 115.
5 D. Di Carlo, K.-H. Jeong and L. P. Lee, *Lab Chip*, 2003, **3**, 287.
6 D. Di Carlo, C. Ionescu-Zanetti, Y. Zhang, P. Hung and L. P. Lee, *Lab Chip*, 2005, **5**, 171.
7 J. Kim, S. Hee Jang, G. Jia, J. V. Zoval, N. a Da Silva and M. J. Madou, *Lab Chip*, 2004, **4**, 516.
8 B. Gabriel and J. Teissié, *Biophys. J.*, 1999, **76**, 2158.
9 F. Han, Y. Wang, C. E. Sims, M. Bachman, R. Chang, G. Li and N. L. Allbritton, *Anal. Chem.*, 2003, **75**, 3688.
10 K. R. Rau, P. a Quinto-Su, A. N. Hellman and V. Venugopalan, *Biophys. J.*, 2006, **91**, 317.
11 H. Zhang and W. Jin, *J. Chromatogr., A*, 2006, **1104**, 346.
12 J. Kim, M. Johnson, P. Hill and B. K. Gale, *Integrative biology : quantitative biosciences from nano to macro*, 2009, **1**, 574.
13 S.-S. Yun, S. Y. Yoon, M.-K. Song, S.-H. Im, S. Kim, J.-H. Lee and S. Yang, *Lab Chip*, 2010, **10**, 1442.
14 B. Wen, J. Sader and J. Boland, *Phys. Rev. Lett.*, 2008, **101**, 2.
15 J. Kim, Z. Li and I. Park, *Lab Chip*, 2011, **11**, 1946.
16 L. E. Greene, B. D. Yuhas, M. Law, D. Zitoun and P. Yang, *Inorg. Chem.*, 2006, **45**, 7535.
17 S. Satyanarayana, R. N. Karnik and A. Majumdar, *J. Microelectromech. Syst.*, 2005, **14**, 392.